NJC

Accepted Manuscript

ROYAL SOCIETY OF CHEMISTRY

www.rsc.org/njc

MOLECULAR-ENGINEERED [Ir(*Fppy*)$_2$(*Mepic*)] TOWARDS EFFICIENT BLUE-EMISSION

Kassio P.S. Zanoni [1], *Akitaka Ito* [2] *and Neyde Y. Murakami Iha* [1*]

[1]Laboratory of Photochemistry and Energy Conversion, Departamento de Química Fundamental, Instituto de Química, Universidade de São Paulo – USP, Av. Prof. Lineu Prestes, 748, 05508-900, São Paulo, SP, Brazil; E-mail: neydeiha@iq.usp.br,

[2]Department of Chemistry, Graduate School of Science, Osaka City University, 3-3-138 Sugimoto, Sumiyoshi-ku, Osaka 558-8585, Japan.

Keywords: Iridium Complex; Molecular Engineering; CIE Coordinates; TD-DFT; Franck-Condon Analysis.

ABSTRACT

A novel Ir(III) complex, [Ir(*Fppy*)$_2$(*Mepic*)] (*Fppy* = 2-(2,4-difluorophenyl)pyridinate; *Mepic* = 3-methylpyridine-2-carboxylate) was engineered to show a blue phosphorescence with an impressive unitary quantum yield in our search for luminescent metal complexes for low cost displays and efficient lighting devices. Application of the Golden Rule through Franck-Condon spectral analyses along with TD-DFT calculations and comparisons to the [Ir(*Fppy*)$_2$(*pic*)] complex have provided insights on the mixing extension between charge-transfer (CT) and ligand-centered (LC) excited states in the emissive lowest-energy triplet transition for different media. The relatively narrow and vibronically-structured emission of [Ir(*Fppy*)$_2$(*Mepic*)] at 298 K mainly arises from a spin–orbit-induced mixed $^3\mathrm{MLCT\text{-}LC}_{\mathrm{Ir}(Fppy)\rightarrow Fppy}/^3\mathrm{LLCT}_{Fppy\rightarrow Mepic}$ excited state, with an enhanced MLCT character because of the methyl addition to *pic*. In a frozen media at 77 K, the CT contribution is extinguished, leading to a pure LC_{Fppy} emission, with similar emissive spectral profile to the free ligand, *FppyH*. The efficient

blue emission shows that the complex is suitable for high-performance light-emitting devices and for thermo- and rigidity-sensors.

TABLE OF CONTENTS ENTRY

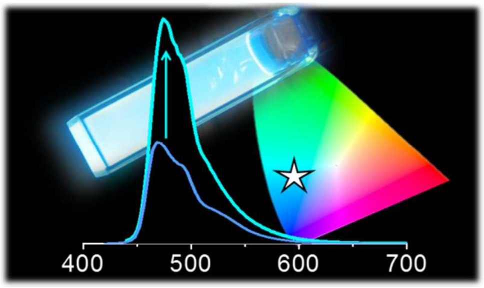

TABLE OF CONTENTS SYNOPSIS

A detailed photophysical investigation of [Ir(*Fppy*)$_2$(*Mepic*)] by TD-DFT and Frank-Condon emission band shape analyses revealed a succeeded molecular engineering towards an intensified blue emission, with phosphorescence from a spin–orbit-induced mixed ^{3}MLCT-LC$_{Ir(Fppy)\rightarrow Fppy}$/^{3L}LCT$_{Fppy\rightarrow Mepic}$ excited state and an impressive unitary quantum yield.

INTRODUCTION

Worldwide concerns for increasing energy demand significantly spur the scientific endeavor for novel efficient lightening technologies. One of the most successful, low-consumption and eco-friendly technologies are the organic light-emitting diodes (OLEDs), typically prepared by vacuum processes in a multilayered structure.[1-6] In the emitting layer of OLEDs, both host matrix and guest emissive species play important roles. The former promotes formation of excited state of the guest species by energy transfer. Since the innovative work by Forrest and Thompson in 1998,[7] phosphorescent transition metal complexes have been broadly utilized as guests in order to achieve high external conversion efficiencies, since their emitting triplet states harvest both singlet (25 %) and triplet excitation (75 %).[2,6,7,8] In special, Ir(III) complexes are the most prominent due to their strong structural and electronic interactions between ligand(s) and the metal center with one of the highest spin–orbit coupling (SOC) constant (i.e. $\xi_{\mathrm{Ir}} = 4430\ \mathrm{cm}^{-1}$).[5,9,10] These facts lead to remarkable and unique features, such as excellent thermal and photochemical stability and the tunability of absorption and emission spectra as well as redox potentials.[11-14]

Several works have emerged concerning the efficiency and color versatility of Ir(III)-emitters.[1,2,4,10] The luminescence of cyclometalated Ir(III) complexes is best ascribed as pertaining to an admixture of MLCT and LC states.[1,15,16] Two of the main synthetic strategies to increase quantum yields of Ir(III) emitters[10] are to limit the emission within only one appropriate ligand[17,18,19] and induce a larger mixing between MLCT and LC states.[20,21,22] The addition of a methyl group to the *Fppy* moiety of $[\mathrm{Ir}(Fppy)_2(NN)]$ complexes, for example, led to increases in radiative rates by enhancing the MLCT character in the emissive state, yet no major impacts in their emission energies were observed.[23]

In our previous work,[22] emission properties of a series of heteroleptic Ir(III) complexes, $[\mathrm{Ir}(Xppy)_2(NN)]^+$ (*Xppy* = cyclometalated ligands; *NN* = diimine ligands), with luminescence from orange to blue-green, were quantitatively evaluated to provide the extent of coupling between $^3\mathrm{MLCT}_{\mathrm{Ir(ppy)}\rightarrow NN}$ and $^3\mathrm{LC}_{NN}$ states, which drastically enhanced the emission quantum yield. One of these complexes, $[\mathrm{Ir}(ppy)_2(dmb)]^+$ (*ppy* = 2-phenylpyridinate; *dmb* = 4,4'-dimethyl-2,2'-bipyridine), was also successfully used as the active layer in a light emitting electrochemical cell (LEC).[24]

In this work, a blue light-emissive Ir(III) complex, $[\mathrm{Ir}(Fppy)_2(Mepic)]$, **FIrMepic** (*Fppy* = 2-(2,4-difluorophenyl)pyridinate and *Mepic* = 3-methylpyridine-2-carboxylate), was engineered by introduction of a methyl group to the picolinate moiety of the $[\mathrm{Ir}(Fppy)_2(pic)]$, **FIrpic,** archetypal-blue-emitter[25] to enhance the MLCT character in the triplet emissive state. The intense phosphorescence of the designed complex and the distinct photophysical properties are discussed in details, with results supported by experimental and theoretical techniques, such as state-of-the-art Franck-Condon analyses for the emission spectra and time-dependent density function theory (TD-DFT) calculations.

EXPERIMENTAL SECTION

All chemicals and solvents for synthesis were purchased from Sigma-Aldrich or Synth, and used as supplied. HPLC grade acetonitrile, propionitrile or butyronitrile were used for the spectroscopic and photophysical measurements. Compounds *mer*-[Ir(*Fppy*)$_2$(*dmb*)][PF$_6$] and *fac*-[Ir(*ppy*)$_3$], employed as emission standards for the emission quantum yield measurement, were synthesized as previously described,[22,26] while [Ru(*bpy*)$_3$]Cl$_2$ was purchased from Sigma-Aldrich. The standard complex **FIrpic**, without the methyl group, was synthesized following the same methodology for **FIrMepic** described below.

Synthesis of bis[2-(2,4-difluorophenyl)pyridinate-C^2,N](3-Methylpyridine-2-carboxylate-O,N)iridium(III) (**FIrMepic**)

$IrCl_3 \cdot H_2O$ (400 mg, 1.34 mmol) and 2-(2,4-difluorophenyl)pyridine (*FppyH*, 450 μL, 3.01 mmol) were dissolved in a 3/1 (v/v) mixture of ethylene glycol monoethyl ether/water (20 mL) and heated at reflux with stirring for 10 h. After cooling to room temperature, 3-methylpyridine-2-carboxylic acid (*MepicH*, 200 mg, 1.46 mmol) and Na_2CO_3 (204 mg) were added to the mixture, which was refluxed again for 15 h, leading to an orange solution. The product precipitated upon cooling was collected by filtration, and washed three times with ultra-pure water then diethyl ether. The yellow solid was recrystallized by dissolving the solid in ethyleneglycol monoethylether and precipitated adding water slowly. The product, Chart 1, was filtrated, washed with diethyl ether and dried under vacuum to obtain 252 mg of pure product (0.36 mmol, 53% yield).

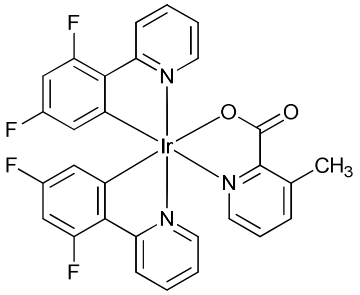

Chart 1. Chemical structure of **FIrMepic**.

Elemental analysis data were obtained on a Perkin-Elmer CHN 2400: Calcd for $IrC_{29}H_{18}N_3O_2F_4{\cdot}2H_2O$: C, 46.67 %; H, 2.98 %; N, 5.64 %. Found: C, 46.61 %; H, 2.95 %; N, 5.68. The ^1H NMR spectrum (Figure S1 and Table S1 in supporting information) was recorded in a 500 MHz Bruker AIII, using CD_3CN as solvent. The residual solvent signal was employed as an internal standard. δ/ppm: 8.61 (1H, d, J = 5.8 Hz), 8.30 (1H, d, J = 8.5 Hz), 8.22 (1H, d, J = 8.3 Hz), 7.91 (1H, t, J = 7.6 Hz), 7.86 (1H, t, J = 7.7 Hz), 7.78 (1H, d; J = 7.6 Hz), 7.63 (1H, d, J = 5.3 Hz), 7.60 (1H, d, J = 5.8 Hz), 7.27 (2H, m), 7.12 (1H, t, J = 5.8 Hz), 6.52 (2H, m), 5.76 (1H, dd, J = 8.9, 2.4 Hz), 5.55 (1H, dd, J = 8.9, 2.4 Hz), 2.72 (3H, s).

Photophysical measurements

UV-Vis absorption spectrum was recorded on an Agilent 8453 diode array spectrophotometer. Steady-state emission spectra were recorded in a PC1 photon-counting spectrofluorimeter (ISS) with a photomultiplier based, photon-counting detector with detector sensitivity correction. Emission decays were recorded on a ChronosBH time-resolved fluorometer (ISS) using a diode laser (λ_{ex} = 378 nm, frequency = 20 kHz, ISS) as an excitation light source. The absorbances at the excitation wavelength of sample solutions were set between 0.1 and 0.2 in four-polished-face quartz cuvettes with 1.000 cm optical path length. Solutions were deoxygenated with argon for at least 10 minutes prior to measurement. For 77 K experiments, samples were prepared in a mixture of propionitrile and butyronitrile (4/5, v/v) (prop:but) in quartz tubes inserted into a quartz Dewar flask containing liquid N_2.

The emission quantum yields (ϕ) for **FIrMepic** and **FIrpic** in acetonitrile at 298 K were calculated by the absolute method applying the methodology developed by Friend et al[27] using a $BaSO_4$-coated integration sphere, Edinburgh 1-M-2 (in the University of North Carolina), as well as by the relative method using Equation 1. For the latter one, acetonitrile solutions of three different reference compounds were employed as emission standards: a) *mer*-[Ir(*Fppy*)$_2$(*dmb*)][PF$_6$] ($\phi = 0.96$ [22], λ_{ex} = 375 nm, with a 389 nm long pass filter); b) [Ru(*bpy*)$_3$]Cl$_2$ ($\phi = 0.094$ [28], λ_{ex} = 400 nm, with a 420 nm long pass filter); c) *fac*-[Ir(*ppy*)$_3$] ($\phi = 0.99$ [29], λ_{ex} = 370 nm, with a 389 nm long pass filter). The results using the integrating sphere and the three references gave excellent agreement.

$$\phi_{Ir} = \phi_{ref} \frac{P_{Ir}}{P_{ref}} \frac{A_{ref}}{A_{Ir}} \qquad (1)$$

ϕ_{Ir} = Emission quantum yield for the sample;

ϕ_{ref} = Emission quantum yield for the reference in the same solvent;

A_{Ir} = Absorbance of the sample at the excitation wavelength;

A_{ref} = Absorbance of the reference at the excitation wavelength;

P_{Ir} = Integral of the sample phosphorescence spectrum;

P_{ref} = Integral of the reference phosphorescence spectrum.

Cyclic Voltammetry measurements were performed with a Gamry Interface 1000 potentiostat. The three-electrode setup consisted of a platinum working electrode (0.5 cm^2), a platinum coiled-wire counter-electrode and a silver wire pseudo-reference. Tetra-*n*-butylammonium hexafluorophosphate (50 mmol L^{-1}) was employed as a supporting electrolyte in acetonitrile and ferrocene (0.3 mmol L^{-1}) as an internal standard ($E^{0}_{\mathrm{Fc/Fc^{+}}}$ = +0.64 V *vs*. NHE).

Theoretical calculations

Molecular orbital calculations for the complex were conducted with a Gaussian 09W software.[30] Optimization of the ground-state geometry was performed by using DFT with the B3LYP functional. The LanL2DZ[31-33] and 6-31G(d,p)[34,35] basis sets were used to treat iridium and all other atoms, respectively. TD-DFT calculations were then performed to estimate energies and oscillator strengths of the lowest-energy 40 singlet and 5 triplet transitions. All the calculations were carried out in acetonitrile as solvent by using a Polarizable Continuum Model (PCM).[36,37] Electron density populations were plotted using GaussView 5.0.[38] The simulated absorption spectrum was generated using the same software.

Franck-Condon analyses for emission spectra

Franck-Condon band shape analyses for emission spectra were carried out on the basis of Equations 2 and 3, which include two and three vibrational acceptor mode(s), respectively, as averages of the multiple modes coupled to the transition between the emitting excited state and the ground state.[39-43] Prior to the spectral fitting analysis, the number of photons at a given wavelength were corrected to the wavenumber scale by using the relationship,[44] $I(\tilde{\nu}) = I(\lambda) \times \lambda^2$.

$$I(\tilde{\nu}) = \sum_{v_{\mathrm{H}}=0}^{\infty}\sum_{v_{\mathrm{L}}=0}^{\infty}\left(\frac{E_0 - v_{\mathrm{H}}\hbar\omega_{\mathrm{H}} - v_{\mathrm{L}}\hbar\omega_{\mathrm{L}}}{E_0}\right)^4\left(\frac{{S_{\mathrm{H}}}^{v_{\mathrm{H}}}}{v_{\mathrm{H}}!}\right)\left(\frac{{S_{\mathrm{L}}}^{v_{\mathrm{L}}}}{v_{\mathrm{L}}!}\right) \times \exp\left[-4\ln 2\left(\frac{\tilde{\nu}-E_0+v_{\mathrm{H}}\hbar\omega_{\mathrm{H}}+v_{\mathrm{L}}\hbar\omega_{\mathrm{L}}}{\tilde{\nu}_{1/2}}\right)^2\right] \quad (2)$$

$$I(\tilde{\nu}) = \sum_{v_{\mathrm{H}}=0}^{\infty}\sum_{v_{\mathrm{M}}=0}^{\infty}\sum_{v_{\mathrm{L}}=0}^{\infty}\left(\frac{E_0 - v_{\mathrm{H}}\hbar\omega_{\mathrm{H}} - v_{\mathrm{M}}\hbar\omega_{\mathrm{M}} - v_{\mathrm{L}}\hbar\omega_{\mathrm{L}}}{E_0}\right)^4\left(\frac{{S_{\mathrm{H}}}^{v_{\mathrm{H}}}}{v_{\mathrm{H}}!}\right)\left(\frac{{S_{\mathrm{M}}}^{v_{\mathrm{M}}}}{v_{\mathrm{M}}!}\right)\left(\frac{{S_{\mathrm{L}}}^{v_{\mathrm{L}}}}{v_{\mathrm{L}}!}\right) \times \exp\left[-4\ln 2\left(\frac{\tilde{\nu}-E_0+v_{\mathrm{H}}\hbar\omega_{\mathrm{H}}+v_{\mathrm{M}}\hbar\omega_{\mathrm{M}}+v_{\mathrm{L}}\hbar\omega_{\mathrm{L}}}{\tilde{\nu}_{1/2}}\right)^2\right] \quad (3)$$

In these equations, $I(\tilde{\nu})$ is the emission intensity at the energy $\tilde{\nu}$ (in cm^{-1}). E_0 is the energy gap between the zeroth vibrational levels in the ground and excited states. $\hbar\omega_\text{H}$, $\hbar\omega_\text{M}$ and $\hbar\omega_\text{L}$ are the quantum spacings for averaged high-, medium- and low-frequency vibrational modes, respectively.[39] S_H, S_M and S_L are the associated electron-vibrational coupling constants or Huang-Rhys factors,[45] related to structural differences between excited and ground states along the displacement normal coordinates of the coupled average high-, medium- and low-frequency vibrational modes, respectively. $\tilde{\nu}_{1/2}$ is the full width at half-maximum (fwhm) for an individual vibronic line.[46,47] In the fitting procedure, E_0, $\hbar\omega$, S and $\tilde{\nu}_{1/2}$ were optimized with a least-squares minimization routine with application of a Generalized Reduced Gradient (GRG2) algorithm.[48] The summation was carried out from $v^* = 0$ in the excited state to levels $v = 0 \rightarrow 10$ (for 2-mode fit) or 0→5 (for 3-mode fit) in the ground state.

RESULTS AND DISCUSSION

Absorption

The electronic absorption spectrum of **FIrMepic** in acetonitrile at 298 K is shown in Figure 1, along with the simulated spectrum, which are similar to those of parent complexes, $[\text{Ir}(\textit{Fppy})_2(\textit{dmb})]^+$ or **FIrpic**.[22,25,49] The major band around 253 nm can be ascribed to a ligand-centered (LC) ππ* transition in the *Fppy* ligand(s). Broad and relatively weak absorptions observed in the longer wavelength region are an overlap of LC, metal-to-ligand charge transfer (MLCT) and ligand-to-ligand charge transfer (LLCT) mixed-spin transitions as a direct consequence of the strong SOC effect exerted by the Ir(III) core:[1,9,10,15,22] for instance, the less intense lowest-lying band around 460 nm is ascribed to a spin-forbidden triplet transition. Although it is difficult to assign the nature of this featureless absorption, TD-DFT calculations and photophysical properties (i.e., τ, k_nr and k_r) lead to a mixed MLCT/LC excited state, which is *Fppy*-related since

Mepic-related ones lye at higher energies.[51] This mixed MLCT/LC excited state corresponds to an intramolecular charge transfer transition from a $d\pi_{Ir(Fppy)}$ to a π^*_{Fppy}-orbital enabled by the strong quasi-covalent bond between Ir(III) and C atoms in the *Fppy* ligands.

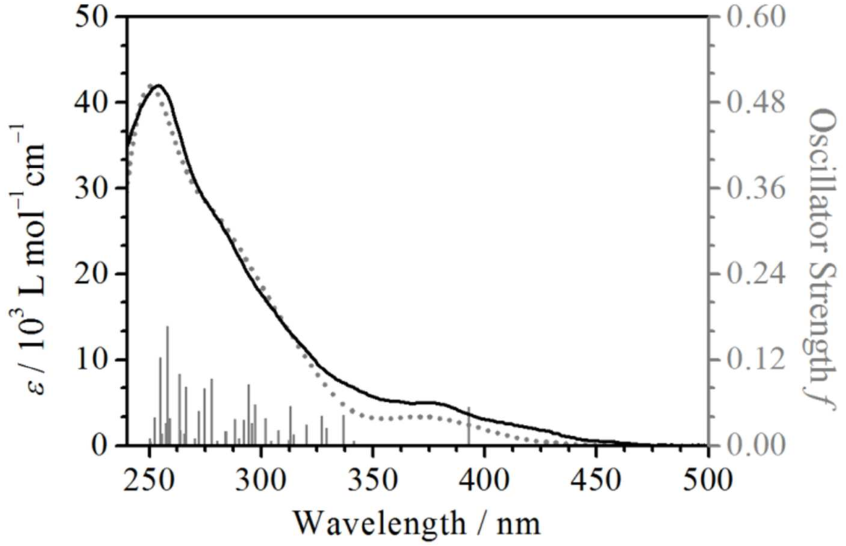

Figure 1. Electronic absorption spectrum of **FIrMepic** (black —) and the simulated spectrum by TD-DFT calculations (grey •••), both in acetonitrile at 298 K.

TD-DFT calculated energies and oscillator strengths for singlet transitions of **FIrMepic** are correlated with the experimental absorption spectrum, Figure 1, by assuming full widths at half-maximum of the transitions to be 0.230 eV and shifting the spectrum to higher-energy by 5%. Slight deviations observed in the low-energy region are due to the contributions of spin-orbit-allowed triplet transitions which are not taken in account in the simulation.

Table 1 summarizes related molecular orbitals (MOs) for singlet (S_1–S_{10}) and triplet (T_1) transitions, with energies corrected by the 5% factor. The three lowest-energy singlet transitions (S_1, S_2 and S_3) result from several MOs mainly related to the highest-energy occupied MO (HOMO), characterized as $d\pi_{Ir(\mathit{Fppy})}$. From electron density populations and contours in Table 2 and Figure 2, the lowest-energy unoccupied MO (LUMO) and LUMO+2 are best characterized as π*-orbitals of the *Fppy* ligand and LUMO+1 is of the *Mepic* ligand. Therefore, S_1 to S_3 transitions are mainly ascribed to $MLCT_{Ir\rightarrow \mathit{Fppy}}$ and $MLCT_{Ir\rightarrow \mathit{Mepic}}$ having partial mixing with LC_{Fppy} and $LLCT_{\mathit{Fppy}\rightarrow \mathit{Mepic}}$, respectively. The nature of HOMO for **FIrMepic** is very similar to those of the related complexes, $[Ir(\mathit{Fppy})_2(\mathit{dmb})]^+$ and **FIrpic**.[22,25,49] The S_4 to S_7 transitions are mainly originated from HOMO–1 ($d\pi_{Ir(\mathit{Fppy})}$) and mixed-MOs.

The calculated S_1 energy (E_{S1} = 3.156 eV) for **FIrMepic** is in very-good agreement to the experimental electrochemical data in acetonitrile (ΔE_{REDOX} = 3.2 V), from oxidation and reduction potentials around 1.5 and -1.7 V *vs.* NHE, respectively, similarly to **FIrpic** (1.6 and -1.7 V, ΔE_{REDOX} = 3.21 V).[25]

Table 1. Energies and contributions of individual MOs for transitions in the **FIrMepic** complex.

Excited State	Energy* (Wavelength)	Transition
S_1	3.156 eV (393 nm)	HOMO–0 → LUMO+0 (61 %) HOMO–0 → LUMO+1 (39 %)
S_2	3.224 eV (385 nm)	HOMO–0 → LUMO+1 (80 %) HOMO–0 → LUMO+2 (20 %)
S_3	3.271 eV (379 nm)	HOMO–0 → LUMO+2 (82 %) HOMO–0 → LUMO+0 (18 %)
S_4	3.632 eV (341 nm)	HOMO–1 → LUMO+0 (40 %) HOMO–1 → LUMO+1 (36 %) HOMO–1 → LUMO+2 (24 %)
S_5	3.681 eV (337 nm)	HOMO–1 → LUMO+0 (81 %) HOMO–2 → LUMO+1 (19 %)
S_6	3.768 eV (329 nm)	HOMO–1 → LUMO+2 (56 %) HOMO–0 → LUMO+3 (44 %)
S_7	3.790 eV (327 nm)	HOMO–0 → LUMO+3 (81 %) HOMO–1 → LUMO+1 (19 %)
S_8	3.872 eV (320 nm)	HOMO–2 → LUMO+0 (40 %) HOMO–4 → LUMO+0 (24 %) HOMO–3 → LUMO+0 (23 %) HOMO–2 → LUMO+1 (13 %)
S_9	3.943 eV (314 nm)	HOMO– → LUMO+4 (100%)%)
S_{10}	3.960 eV (313 nm)	HOMO–2 → LUMO+2 (20 %) HOMO–0 → LUMO+4 (19 %) HOMO–2 → LUMO+0 (18 %) HOMO–4 → LUMO+2 (13 %) HOMO–3 → LUMO+2 (11 %) HOMO–3 → LUMO+0 (10 %) HOMO–4 → LUMO+0 (09 %)
T_1	2.830 eV (438 nm)	HOMO–0 → LUMO+0 (53 %) HOMO–0 → LUMO+1 (34 %) HOMO–3 → LUMO+2 (13 %)

*Energy values were shifted to higher-energy by 5%.

Table 2. MO electron density populations for S_1 to S_7 and T_1 transitions in the **FIrMepic** complex.

	Molecular Orbital	**Contribution / %**		
		Ir(III)	***Fppy***	***Mepic***
Triplet	LUMO+2	2.43	3.89	**93.68**
	LUMO+1	5.10	**91.93**	2.97
	LUMO	5.97	**90.39**	3.64
Singlet	LUMO+3	2.78	**64.11**	33.11
	LUMO+2	5.19	**88.27**	6.54
	LUMO+1	5.29	35.27	**59.44**
	LUMO	2.71	**65.09**	32.20
	HOMO	**50.22**	43.59	6.19
	HOMO-1	**56.66**	27.18	16.16
	HOMO-2	29.73	**65.83**	4.44
	HOMO-3	23.09	**68.61**	8.30

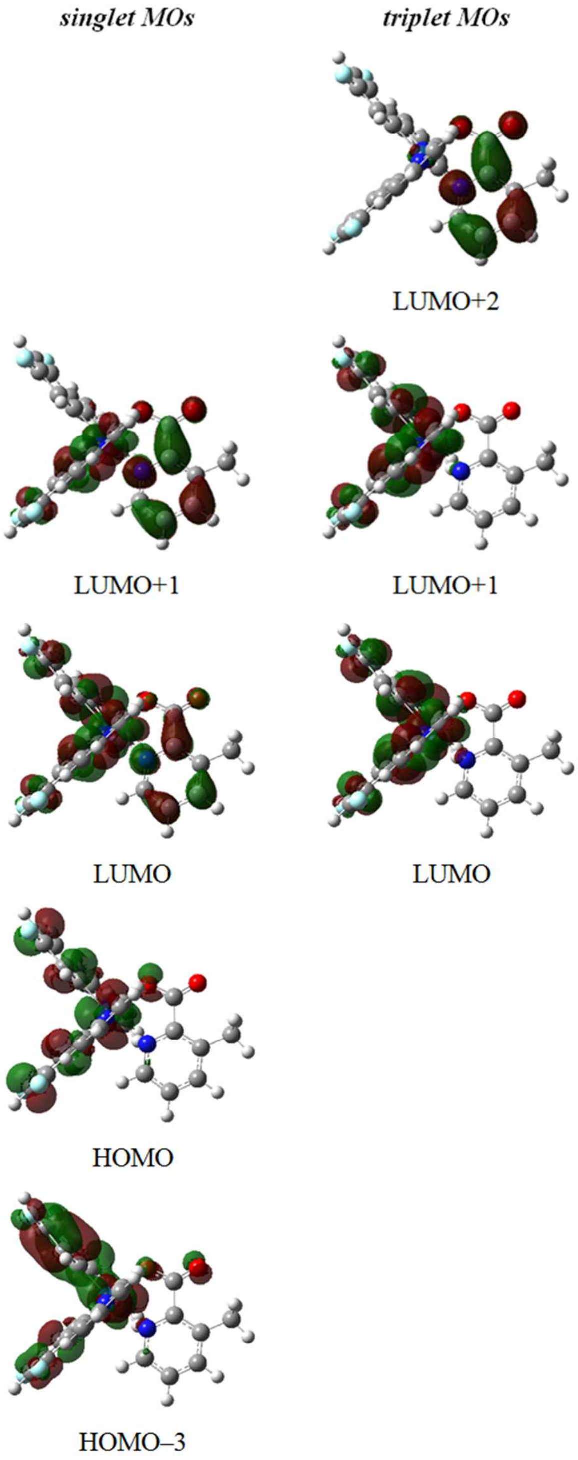

Figure 2. MO contours (0.03 eÅ^{-3}) related to S_1 and T_1 transitions in **FIrMepic**.

Emission at 298 K

Excitation of **FIrMepic** in acetonitrile at 298 K leads to singlet (and triplet) excited states, followed by internal conversion and intersystem crossing to give the lowest-lying triplet state (T_1). MOs of T_1 differ from those of the relevant singlet state, Figure 2 and Table 2. The excitation spectrum, Figure 3, is almost identical to the absorption spectrum in the 270–465 nm region, Figure 1, and indicative of an efficient formation of the T_1 state. Deviations in the 230–270 nm region are due to the inner filter effect.

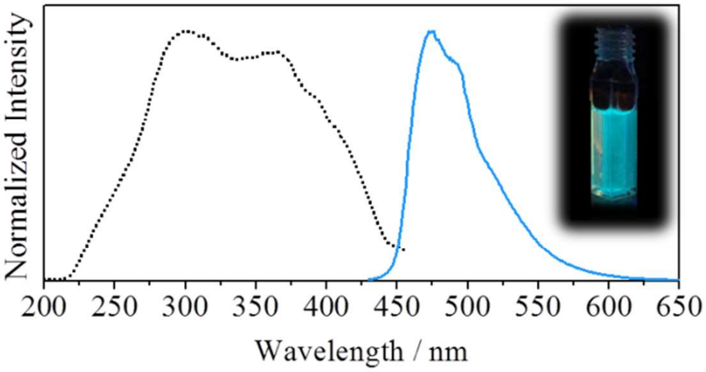

Figure 3. Excitation (black ••••; λ_{em} = 474 nm) and emission spectra (blue —; λ_{ex} = 365 nm) for [Ir(*Fppy*)$_2$(*Mepic*)] in acetonitrile at 298 K.

Deactivation from T_1 occurs with intense blue phosphorescence and the emission spectrum is relatively narrow with weak vibronic modes, Figure 3. The emission maximum at 474 nm in acetonitrile, Table 3, is almost independent of the polarity of the surrounding medium, as shown in Figure S2 in supporting information. The methyl group in the *pic* moiety has a little influence on λ_{max} (compared to **FIrpic**) and only plays a major role in the emissive constant, as discussed in following paragraphs.

The uncoordinated *FppyH* ligand exhibits a weak $^{1}\pi\pi^{*}{}_{Fppy}$-fluorescence at 298 K ($\lambda_{\max}$ = 307 nm), whereas the $^{3}\pi\pi^{*}{}_{Fppy}$-phosphoresnce is only observed at frozen media at 77 K, ($\lambda_{\max}$ = 455 nm), Figure S7 in supporting information. The structured and media-independent emission for the **FIrMepic** could indicate a $\pi\pi^{*}$-based character of T_1 state related to *Fppy* ligands. In this assumption, the heavy Ir(III) core acts solely on eliminating the forbidden character of intersystem crossings, which leads to the phosphorescence from the lowest-lying $^{3}\pi\pi^{*}{}_{Fppy}$ channel. However, the impressively high emission quantum yield ($\phi \sim 1$) and the relatively long-lived emission (τ = 0.76 μs) for the complex at 298 K, Table 3, differs significantly from those for pure $\pi\pi^{*}$ phosphorescence in same conditions and are analogous to pure ^{3}MLCT emissions.[15,43,52-54] Therefore, from the distinct emission properties, it is more appropriate to assume a mixed MLCT-LC character (*Fppy*-based) for the T_1 state of **FIrMepic**, harvested by singlet and triplet relaxations, similarly to **FIrpic** (Figure S8 in supporting information).

Table 3. Emission properties of **FIrMepic**, **FIrpic** and the free *FppyH* ligand in different media at 298 and 77 K.

Compound	Media		$\lambda_{\max}$ (nm)	ϕ^{*}	τ (μs)	k_r (10^5 s^{-1})	k_{nr} (10^4 s^{-1})
FIrMepic	Acetonitrile	298 K	474	0.98 ± 0.02[a] 0.96 ± 0.06[b] 0.98 ± 0.05[c] 0.96 ± 0.05[e]	0.77	13	2.6
	prop:but	298 K	472	**	0.61	--	--
		77 K	456	**	1.97	--	--
FIrpic	Acetonitrile	298 K	470	0.80 ± 0.03[c] 0.83 ± 0.07[d]	0.74	11	2.3
	prop:but	77 K	456	**	1.95	--	--
FppyH	Acetonitrile	298 K	307	< 0.005	**	--	--
	prop:but	77 K	455	**	1.90	--	--

*Quantum yields were measured by the relative method against standard compounds - *mer*-[Ir($Fppy$)$_2$(dmb)][PF$_6$] [22] (a), [Ru(bpy)$_3$]Cl$_2$ [28] (b), *fac*-[Ir(ppy)$_3$] [29] (c), or the **FIrMepic** sample itself (d) - or by the absolute method using an integrating sphere (e).
**Not measured.

Emission quantum yields for **FIrMepic**, Table 3, were measured by the relative method against three different emission standards to verify the impressive obtained values: a) *mer*-[Ir(*Fppy*)$_2$(*dmb*)][PF$_6$] [22]; b) [Ru(*bpy*)$_3$]Cl$_2$ [28]; c) *fac*-[Ir(*ppy*)$_3$] [29]. Data obtained using the three standards are in excellent agreement among them and also to the absolute value, measured using an integrating sphere. Indeed, **FIrMepic** shows an unitary quantum yield, higher than **FIrpic**, and the electronic origins for the emission-enhancement are explained in following paragraphs. Here, it is worth reinforcing that the ϕ values for **FIrpic** obtained in this work (0.83 and 0.80) are considerably higher compared to previews measurements (0.63 [55] or 0.61[11] in the same solvent). This value is very accurate considering it was obtained using two more-appropriate reference compounds (with similar λ_{em}, λ_{exc} and ϕ [56]), whose quantum yields were also previously measured by an integrating sphere. The use of the reevaluated value can avoid misleading comparisons in future works.

It is clear that the T$_1$ state of **FIrMepic** mainly deactivates through a radiative process (k_{r}), Table 3, rather than the nonradiative one (k_{nr}), both calculated by Equations 4a and 4b.

$$\phi = \frac{k_{\mathrm{r}}}{k_{\mathrm{r}} + k_{\mathrm{nr}}} \tag{4a}$$

$$\tau = \frac{1}{k_{\mathrm{r}} + k_{\mathrm{nr}}} \tag{4b}$$

k_{r} is related to the square of the transition dipole moment upon radiative deactivation from the mixed-T$_1$ state,[1,22,50] resultant from the SOC-permutation between close- and low-lying excited states of different nature.[1,9,10,22,50] The remarkable k_{r} value (13×10^5 s^{-1}) for **FIrMepic** is an experimental proof of the mixed-nature for T$_1$ with a major role of a stronger-dipole MLCT counterpart, similarly to that of [Ir(*Fppy*)$_2$(*dmb*)]$^+$ ($k_{\mathrm{r}} = 15 \times 10^5$ s^{-1}).[22]

A mixed character for T_1 at 298 K is also supported by TD-DFT calculations. As summarized in Table 1, the lowest-lying triplet excited state is ascribed to an interaction between three different transitions, HOMO → LUMO (53%), HOMO → LUMO+1 (34%) and HOMO-3 → LUMO+2 (13%). The first two are similar in nature (both triplet-LUMO and triplet-LUMO+1 are π^*_{Fppy} related, Table 2 and Figure 2), possessing totally 87% contribution in the mixed character, thus the emitting excited state of **FIrMepic** is best characterized as ^{3}MLCT-$LC_{Ir(Fppy)\rightarrow Fppy}$. The third one is assigned to a $^3LLCT_{Fppy\rightarrow Mepic}$ transition, $\pi_{Fppy}\pi^*_{Mepic}$ related, and has a minor contribution (13%) to the emitting T_1 state.

As summarized in Table 2, the observed k_r-constant for **FIrMepic** is higher than **FIrpic** (by 2×10^5 s^{-1}) as a consequence of the methyl addition, although the electronic origin is not obvious and relies on SOC-induced permutations[1,10,50] theoretically corroborated by TD-DFT, as described hereafter. For **FIrpic**, the absence of electron-donating methyl group in the *pic* moiety leads to a more stabilized π^*_{pic} (triplet-LUMO+2) hence a smaller energy difference between $^3LLCT_{Fppy\rightarrow pic}$ and the low-lying ^{3}MLCT-$LC_{Ir(Fppy)\rightarrow Fppy}$ states. This smaller ΔE results in a more effective mixing between the MLCT-LC and LLCT counterparts, decreasing the (stronger-dipole-) MLCT character (80%, Tables S3 and S5 in supporting information) in T_1. Not only the lower MLCT influence but also the LLCT enhancement is hazardous to k_r by weakening of Ir-ligand bonds.[19]

TD-DFT calculations were also conducted for two other possible isomers (*4-* and *5-Mepic*), to analyze theoretically the impact of the methyl position in the resultant T_1 admixture based on the proposed SOC-induced electronic mechanism. Their electron density populations and contours are summarized in Tables S6-S9 and Figures S10-S12 in supporting information. The calculated excited state properties of the 6-*Mepic* isomer (with a reported ϕ value lower than

FIrpic[17,18]) are not compared, since the methyl group distorts the complex structure by a steric hindrance.

A comparison of orbital energies among the three isomers, Tables S6-S9 in Supporting Information, indicates a lower value for the 3-*Mepic* complex (–1.802 eV), which comes from an orbital node exactly at the 3-position that leads to a less effective electron donating effect. Substitution in the 4-position is the most effective (-1,768 eV), since the electron donation occurs in the inverse direction of the Ir(*Fppy)*-to-*Mepic* charge transfer, as similarly observed for the Ru-to-*dmb* charge transfer in the $[\mathrm{Ru}(dmb)_3]^{2+}$ complex.[57-59]

In terms of the final admixture in the T_1 transition, the $^3\mathrm{LLCT}_{Fppy\rightarrow Mepic}$ (HOMO-3 → LUMO+2) influence increases from 3-*Mepic* to 4-*Mepic* complexes (from 13% to 15%), decreasing the contribution of the MLCT counterparts (85% for 4-*Mepic*), Table S10 in supporting information. The MLCT character is further decreased in the 5-*Mepic* complex (69%) by an influence of a fourth transition, LC_{Fppy} related (15%), in the excited state mixing, Table S11 in supporting information. Therefore, based on this proposed electronic effect, it is also possible to speculate that the 4-*Mepic* isomer will lead to a higher emissive constant compared to the non-substituted **FIrPic**, since it also possesses a higher MLCT/LLCT ratio, yet only the 3-*Mepic* one has been synthesized.

As for non-radiative processes, k_{nr} is slightly higher for **FIrMepic** (2.6×10^4 s^{-1}) in comparison to **FIrpic** (2.3×10^4 s^{-1}, here obtained using the new reevaluated ϕ value) as a consequence of its slightly lower-energy emission, in accordance to the energy gap-law that predicts higher k_{nr} constants for decreased emission energies (ln k_{nr} is linear to $-E_{\mathrm{em}}$).[22,39] Nevertheless, the much larger increase in k_{r}, as discussed above, plays a major role in the resultant enhanced quantum yield.

Humans can perceive colors by a trichromatic stimuli on the virtual cortex, quantified by the Comission Internationale d'Eclairage (CIE) in three matching functions or spectral sensitivity curves, $\overline{x}(\lambda)$, $\overline{y}(\lambda)$ and $\overline{z}(\lambda)$.[60,61] The x and y CIE coordinates for **FIrMepic**, **FIrpic** and $[\mathrm{Ir}(Fppy)_2(dmb)]^+$ were calculated by Equations 5a and 5b from their X, Y and Z tristimulus, Equations 6a to 6c, using photoluminescence spectral data in acetonitrile at 298 K. The numerical values of the CIE standard $\overline{x}(\lambda)$, $\overline{y}(\lambda)$ and $\overline{z}(\lambda)$, are available as free-access tables.[62]

$$x = \frac{X}{X+Y+Z} \tag{5a}$$

$$y = \frac{Y}{X+Y+Z} \tag{5b}$$

$$X = \int_{380}^{780} I(\lambda)\bar{x}(\lambda)\mathrm{d}\lambda \tag{6a}$$

$$Y = \int_{380}^{780} I(\lambda)\bar{y}(\lambda)\mathrm{d}\lambda \tag{6b}$$

$$Z = \int_{380}^{780} I(\lambda)\bar{z}(\lambda)\mathrm{d}\lambda \tag{6c}$$

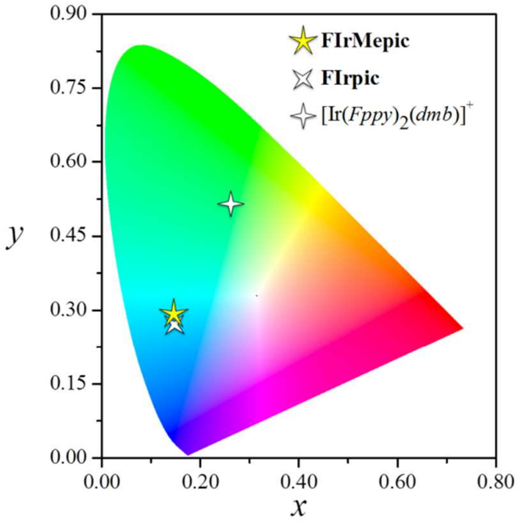

Figure 4. Color space chromaticity diagram with CIE coordinates for the emission of **FIrMepic**, **FIrpic** and $[\mathrm{Ir}(Fppy)_2(dmb)]^+$ in acetonitrile at 298 K.

The emissive deactivation of **FIrMepic** in acetonitrile at 298 K is sky-blue (x = 0.14; y = 0.29), with CIE coordinates practically identical to the standard blue emissive **FIrpic** (x = 0.14; y = 0.26) in same conditions, Figure 4. The remarkable ϕ strenghs this complex to be employed as a standard triplet-emitter and could also be suitable for the pursuit of white-light emitting devices. These results also show our progress from our previously reported bluish-green $[\mathrm{Ir}(Fppy)_2(dmb)]^+$ (x = 0.26; y = 0.52) towards emission in a very attractive and highly desired color even at room temperature.

Emission at 77 K

As for the emission of **FIrMepic** and **FIrpic** in prop:but frozen glasses at 77 K, their spectra are narrower and shifts to higher-energy in comparison to the 298 K one, Figure 5. Their band shapes resemble the phosphorescence from uncoordinated *FppyH* at the same temperature and solvent as well as their emission lifetimes are identical, leading to a pure $^3\mathrm{LC}_{Fppy}$ emission character for both complexes at 77 K. The medium freezing is also followed by an intensity increase for the **FIrpic** complex arising from the temperature dependence of the energy gap law.[22,39]

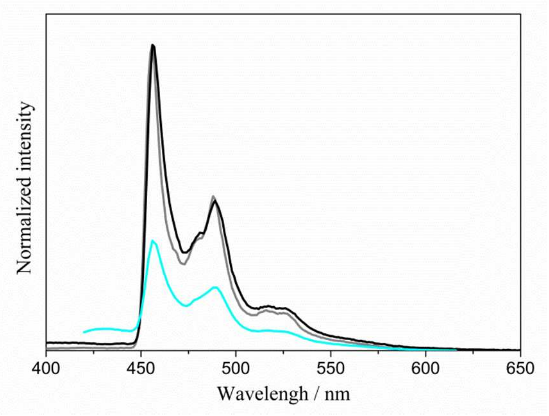

Figure 5. Emission spectra at 77 K (λ_{ex} = 365 nm) for **FIrMepic** (black —), **FIrpic** (grey —) and *FppyH* (cyan —) in prop:but frozen glasses.

Franck-Condon analyses for emission spectra

In order to quantitatively evaluate the excited-state character and vibrational progressions of the emitting T_1 state in different media and temperatures, Franck-Condon analyses for emission spectra were conducted by application of the 2- or 3-average mode approximation, Equations 2 or 3. Fitted spectra for **FIrMepic** are shown in Figure 6, together with the experimentally obtained ones, and the fitting parameters are summarized in Table 4.

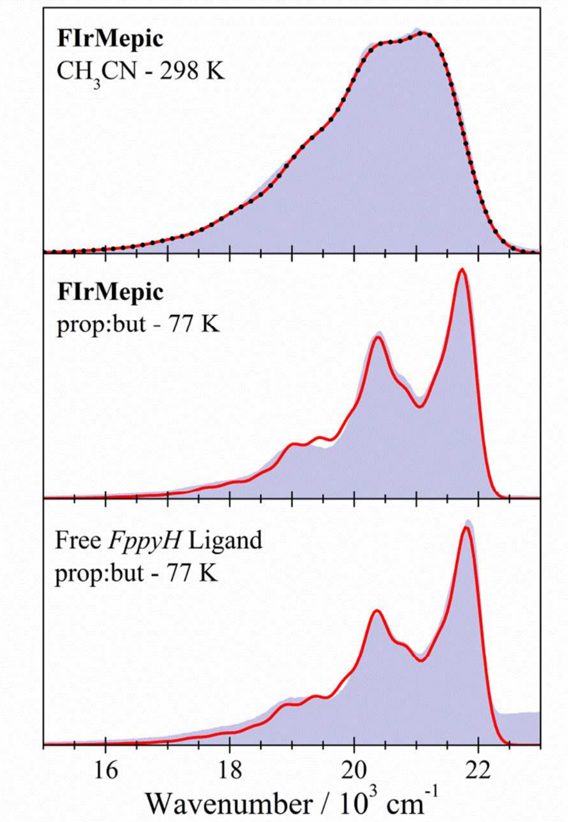

Figure 6. Experimental (solid grey areas) and fitted emission spectra for **FIrMepic** and *FppyH* by using Equations 2 (•••) or 3 (—) and parameters summarized in Table 4.

Table 4. Spectral fitting parameters for **FIrMepic**, **FIrpic** and *FppyH* at 298 (in acetonitrile) and 77 K (in prop:but).

T / K	Compound	Number of vibrational modes	E_0	$\tilde{\nu}_{1/2}$	$\hbar\omega_H$	$\hbar\omega_M$	$\hbar\omega_L$	S_H	S_M	S_L	R
			/ cm^{-1}								
298	**FIrMepic**	2	21300	1110	2240	--	990	0.15	--	1.09	0.9996
		3	21300	1110	2250	1390	980	0.15	0.01	1.09	0.9996
	FIrpic	2	21400	1080	2380	––	1070	0.15	––	1.00	0.9989
		3	21420	1040	2460	1320	980	0.12	0.28	0.79	0.9990
77	**FIrMepic**	3	21880	450	1470	1010	470	0.59	0.38	0.45	0.9969
	Firpic	3	21920	430	1450	1010	490	0.60	0.37	0.39	0.9960
	FppyH	3	21820	490	1470	1000	480	0.58	0.38	0.48	0.9974

The emission spectra of both complexes in nitriles at 298 K were adequately reproduced (correlation factor $R \geq 0.9995$) by accounting high- ($\hbar\omega_H$) and low-frequency ($\hbar\omega_L$) averaged vibrational modes, Equation 2. The **FIrMepic** spectrum is almost independent ($S_M \sim 0.01$) to the medium-frequency mode ($\hbar\omega_M$) obtained by the fitting using Equation 3.

The obtained E_0 for **FIrMepic** at 298 K (21300 cm^{-1}, or 2.64 eV) is in good agreement to the TD-DFT-calculated T_1 energy and it fairly correlates to ΔE_{REDOX} (3.19 V) in a factor of 0.83, very similar to $[Ir(Xppy)_2(NN)]^+$ complexes (0.82),[22] differing from unity because the emission energy also accounts intersystem crossings and contributions from outer and inner-sphere reorganization energies. These are characteristic features of most emitters with a main MLCT nature.[22,63-68]

The $\tilde{\nu}_{1/2}$ (or fwhm) of an individual vibronic line is proportional to the square root of the solvent reorganization energy, with higher values for CT emissions.[39] fwhm obtained for 298 K **FIrMepic** emissions (~ 1100 cm^{-1}) arise from the mixed CT-LC nature, since values are lower than pure CT states (~2580 cm^{-1} - on the basis of two-mode fit [22]), yet not as small as pure LC ones (e.g. the free *FppyH* ligand, ~ 490 cm^{-1}). For **FIrpic**, the lower MLCT character in the mixed-T_1 state results in a slight decrease in fwhm (~ 1040 cm^{-1}).

The medium- and low-frequency modes obtained from the spectral fittings at 298 K ($\hbar\omega_M$ ~ 1400 cm^{-1} and $\hbar\omega_L$ ~ 980 cm^{-1}) can be ascribed to skeletal modes in the *Fppy* ligand since similar frequency modes are obtained from the spectral simulation for *FppyH* (at 77 K). These results are also clear evidences of the *Fppy*-localized T_1 transition in both complexes, as obtained from TD-DFT. The nature of $\hbar\omega_H$ is unclear, possibly a *pic*-skeletal mode associated to the lower $^3LLCT_{Fppy \rightarrow Mepic}$ extent in T_1, since $\hbar\omega_H$ is the most responsive to the addition of the vibration-restrictive methyl-group, with a decrease in frequency from 2460 to 2250 cm^{-1}.

The spectra of both complexes and the free ligand in the frozen media at 77 K are satisfactorily reproduced by the 3-average mode approximation, Equation 3, with quite similar parameters, Table 4. The results clearly demonstrate that the emitting T_1 state of both complexes at 77 K are purely $\pi\pi^*_{Fppy}$ in character (i.e., $^3LC_{Fppy}$) with no extent of MLCT or LLCT mixings, leading to spectral resemblances and comparable emission lifetimes, Table 3. Therefore, by freezing the medium from 298 to 77 K, the mixing of charge-transfer and LC excited states is extinguished by destabilization of CT states owing to pronounced thermo- and rigidochromic effects, in contrast to relatively unaffected ππ* excited states.

CONCLUSIONS

The **FIrMepic** complex was successfully engineered to present desired photophysical features, specially blue luminescence from a distinct-nature excited state. Emission spectrum studies, along with theoretical calculations, have proven a $^3MLCT\text{-}LC_{Ir(Fppy)\rightarrow Fppy}/LLCT_{Fppy\rightarrow Mepic}$ mixed character for the emissive T_1 state of **FIrMepic** and **FIrpic** complexes. Mixed-nature emissive T_1 states are enabled by a strong spin–orbit coupling of the Ir(III) core along with the quasi-covalent bond between Ir(III) and C atoms.

The detailed photophysical study presented here stands as a proof-of-concept example of the interplay between different excited states and SOC-permutations in Ir(III) compounds. Distinct emissive-states lead to very-efficient blue phosphorescence (CIE ~ $x = 0.14$; $y = 0.29$) for both complexes at 298 K, yet the methylated **FIrMepic** complex shows an increased emissive constant, with unitary quantum yield. The electronic origin of this methyl-induced improvement is because of a larger influence of the MLCT counterpart in T_1, based on SOC-induced permutations corroborated by TD-DFT calculations. The influence of the CT-counterpart is extinguished by freezing the medium at 77 K due to a pronounced rigidochromic effect, which leads to a smaller bandwidth in a vibronically-structured spectrum, very similar to that of the free *FppyH* ligand.

The improved photophysical features of **FIrMepic,** in special the unitary quantum yield, makes it a strong candidate for very-efficient light-emitting technologies, such as phosphorescent temperature- and rigidity-sensors, and especially in blue-light emitting devices.

Furthermore, by a judicious device-design, white-light-emitting systems can be developed by employing **FIrMepic** and orange/red Ir(III) complexes within the $x > 0.45$ CIE region (for example, recently published ones[69-72]) in their active layers.

ASSOCIATED CONTENTS

Supporting Information. ^{1}H NMR spectrum of **FIrMepic**, complete TD-DFT data, emission spectra in different media, emission decays and time resolved emission spectrum. This material is available free of charge via the Internet at http://pubs.acs.org.

AUTHOR INFORMATION

Corresponding Author

* E-mail: neydeiha@iq.usp.br

Author Contributions

All authors have given approval to the final version of the manuscript.

Notes

The authors declare no competing financial interest.

AKNOWLEDGEMENTS

This work is supported by Fundação de Amparo à Pesquisa do Estado de São Paulo (FAPESP), and Conselho Nacional de Desenvolvimento Científico e Tecnológico (CNPq). We thank to

Bruna K. Kariyazaki for the initial synthesis of the complex and Dr. M. Kyle Brennaman, from the University of North Carolina at Chapel Hill, for quantum yield absolute measurements.

REFERENCES

1. B. Minaev, G. Baryshnikov, H. Agren, *Phys. Chem. Chem. Phys.,* 2014, **16,** 1719.

2. C.-L. Ho, W.-Y. Wong, *New J. Chem.,* 2013, **37,** 1665.

3. D. Fyfe, *Nature Photon.,* 2009, **3,** 453.

4. C. Ulbricht, B. Beyer, C. Friebe, A. Winter, U.S. Schubert, *Adv. Mater.,* 2009, **21,** 4418.

5. M.S. Lowry, S. Bernhard, *Chem. Eur. J.,* 2006, **12,** 7970.

6. R.C. Evans, P. Douglas, C.J. Winscom, *Coord. Chem. Rev.,* 2006, **250,** 2093.

7. M. Baldo, D. O'Brien, Y. You, A. Shoustikov, S. Sibley, M. Thompson, S. Forrest, *Nature,* 1998, **395,** 151.

8. H. Yersin, A.F. Rausch, R. Czerwieniec, T. Hofbeck, T. Fischer, *Coord. Chem. Rev.,* 2011, **255,** 2622.

9. A.R.G. Smith, P.L. Burn, B.J. Powell, *ChemPhysChem,* 2011, **12,** 2429.

10. Y. You, S.Y. Park, *Dalton Trans.* 2009, **48,** 1267.

11. J. Frey, B.F.E. Curchod, R. Scopelliti, I. Tavernelli, U. Rothlisberger, M.K. Nazeeruddin, E. Baranoff, *Dalton Trans.,* 2014, **43,** 5667.

12. S. Ladouceur, D. Fortin, E. Zysman-Colman, *Inorg. Chem.* 2010, **49,** 5625.

13. F. De Angelis, S. Fantacci, N. Evans, C. Klein, S.M. Zakeeruddin, J.-E. Moser, K. Kalyanasundaram, H.J. Bolink, M. Grätzel, M.K. Nazeeruddin, *Inorg. Chem.,* 2007, **46,** 5989.

14. C. Dragonetti, L. Falciola, P. Mussini, S. Righetto, D. Roberto, R. Ugo, A. Valore, F. De Angelis, S. Fantacci, A.Sgamellotti, M. Ramon, M. Muccini, M., *Inorg. Chem.,* 2007, **46,** 8533.

15. L. Flamigni, A. Barbieri, C. Sabatini, B. Ventura, F. Barigelletti, *Top. Curr. Chem.,* 2007, **81,** 143.

16. M. G. Colombo and H. U. Güdel, *Inorg. Chem.,* 1993, **32,** 3081.

17. Y. You, S.Y. Park, *J. Am. Chem. Soc.*, 2005, **127,** 12438.

18. Y. You, K.S. Kim, T.K. Ahn, D. Kim, S.Y. Park, *J. Phys. Chem. C*, 2007, **111,** 4052.

19. C.J. Chang, C.H. Yang, K. Chen, Y. Chi, C.F. Shu, M.L. Ho, Y.S. Yehc, P.T. Chou, *Dalton Trans.*, **2007,** 1881.

20. J. Li , P.I. Djurovich, B.D. Alleyne, M. Yousufuddin, N.N. Ho, J.C. Thomas, J.C. Peters, R. Bau, M.E. Thompson, *Inorg. Chem.*, **2005,** 44, 1713.

21. A. Tsuboyama, H. Iwawaki, M. Furugori, T. Mukaide, J. Kamatani, S. Igawa, T. Moriyama, S. Miura, T. Takiguchi, S. Okada, M. Hoshino, K. Ueno, *J. Am. Chem. Soc.*, **2003,** 125, 12971.

22. K.P.S. Zanoni, B.K. Kariyazaki, A. Ito, M.K. Brennaman, T.J. Meyer, N.Y. Murakami Iha, *Inorg. Chem.,* 2014, **53,** 4089.

23. S. Ladouceur, K.N.Swanick, S.Gallagher-Duval, Z. Ding, E. Zysman-Colman, *Eur. J. Inorg. Chem.*, 2013, **2013,** 5329.

24. K.P.S. Zanoni, M.U. Sanematsu, N.Y. Murakami Iha, *Inorg. Chem. Commun.,* 2014, **43,** 162.

25. E. Baranoff, B.F.E. Curchod, *Dalton Trans.,* 2015, Advance Article.

26. J. Sun, W. Wu, J. Zhao, *Chem. Eur. J.,* 2012, **18,** 8100.

27. J.C. de Mello, H.F. Wittmann, R.H. Friend, *Adv. Mater.,* 1997, **9,** 230.

28. K. Suzuki, A. Kobayashi, S. Kaneko, K. Takehira, T. Yoshihara, H. Ishida, Y. Shiina, S. Oishi, S. Tobita, *Phys. Chem. Chem. Phys.,* 2009, **11,** 9850.

29. G.J. Barbante, E.H. Doeven, E. Kerr, T.U. Connell, P.S. Donelly, J.M. White, T. Lópes, S. Laird, D.J.D. Wilson, P.J. Barnard, C.F. Hogan, P.S. Francis, *Chem. Eur. J.,* 2014, **20,** 3322.

30. M.J. Frisch, G.W. Trucks, H.B. Schlegel, G.E. Scuseria, M.A. Robb, J.R. Cheeseman, G. Scalmani, V. Barone, B. Mennucci, G.A. Petersson, H. Nakatsuji, M. Caricato, X. Li, H.P. Hratchian, A.F. Izmaylov, J. Bloino, G. Zheng, J.L. Sonnenberg, M. Hada, M. Ehara, K. Toyota, R. Fukuda, J. Hasegawa, M. Ishida, T. Nakajima, Y. Honda, O. Kitao, H. Nakai, T. Vreven, J.A. Montgomery, Jr.; J.E. Peralta, F. Ogliaro, M. Bearpark, J.J. Heyd, E. Brothers, K.N. Kudin, V.N. Staroverov, R. Kobayashi, J. Normand, K. Raghavachari, A. Rendell, J.C. Burant, S.S. Iyengar, J. Tomasi, M. Cossi, N. Rega, N.J. Millam, M. Klene, J.E. Knox, J.B. Cross, V. Bakken, C. Adamo, J. Jaramillo, R. Gomperts, R.E. Stratmann, O. Yazyev, A.J. Austin, R. Cammi, C. Pomelli, J.W. Ochterski, R.L. Martin, K. Morokuma, V.G. Zakrzewski, G.A. Voth, P. Salvador, J.J. Dannenberg, S. Dapprich, A.D. Daniels, Ö. Farkas, J.B. Foresman, J.V. Ortiz, J. Cioslowski, D.J. Fox, *Gaussian 09, Revision A.1*, Gaussian, Inc.: Wallingford CT, 2009.

31. P.J. Hay, W.R. Wadt, *J. Chem. Phys.,* 1985, **82,** 270.

32. W.R. Wadt, P.J. Hay, *J. Chem. Phys.,* 1985, **82,** 284.

33. P.J. Hay, W.R. Wadt, *J. Chem. Phys.,* 1985, 82, 299.

34. A.D. Becke, *J. Chem. Phys.,* 1993, **98,** 5648.

35. C. Lee, W. Yang, R.G. Parr, *Phys. Rev. B,* 1988, **37,** 785.

36. G. Scalmani, M.J. Frisch, *J. Chem. Phys.,* 2010, **132,** 114110.

37. J. Tomasi, B. Mennucci, R. Cammi, *Chem. Rev.* 2005, **105,** 2999.

38. R. Dennington, T. Keith, J. Millam, *GaussView, Version 5*, Semichem Inc: Shawnee Mission KS, 2009.

39. A. Ito, T.J. Meyer, *Phys. Chem. Chem. Phys.* 2012, **14,** 13731.

40. K. Nozaki, K. Takamori, Y. Nakatsugawa, T. Ohno, *Inorg. Chem.,* 2006, **45,** 6161.

41. H.B. Kim, N. Kitamura, S. Tazuke, *J. Phys. Chem.,* 1990, **94,** 7401.

42. G.H. Allen, R.P. White, D.P. Rillema, T.J. Meyer, *J. Am. Chem. Soc.* 1984, **106,** 2613.

43. J.V. Caspar, T.D. Westmoreland, G.H. Allen, P.G. Bradley, T.J. Meyer, W.H. Woodruff, *J. Am. Chem. Soc.* 1984, **106,** 3492.

44. C.A. Parker, W.T. Rees, *Analyst,* 1960, **85,** 587.

45. K. Huang, A. Rhys, *Proc. R. Soc. A,* 1950, **204,** 406.

46. J.T. Hupp, G.A. Neyhart, T.J. Meyer, E.M. Kober, *J. Phys. Chem.,* 1992, **96,** 10820.

47. R.A. Marcus, *J. Phys. Chem.,* 1989, **93,** 3078.

48. D. Fylstra, L. Ladson, J. Watson, A. Waren, *Interfaces,* 1998, **28,** 29.

49. E. Baranoff, B.F.E. Curchod, F. Monti, F. Steimer, G. Accorsi, I. Tavernelli, U. Rothlisberger, R. Scopelliti, M. Grätzel, M.K. Nazeeruddin, *Inorg. Chem.* 2012, **51,** 799.

50. H. Yersin, A. F. Rausch, R. Czerwieniec, T. Hofbeck and T. Fischer, *Coord. Chem. Rev.*, 2011, **255**, 2622.

51. S. Lamansky, P. Djurovich, D. Murphy, F. Abdel-Razzaq, R. Kwong, I. Tsyba, M. Bortz, B. Mui, R. Bau, M.E. Thompson, *Inorg. Chem.,* 2001, **40,** 1704.

52. L.A. Worl, R. Duesing, P. Chen, L.D. Ciana, T.J. Meyer, *J. Chem. Soc., Dalton Trans.,* 1991, 849.

53. A. Juris, V. Balzani, F. Barigelletti, S. Campagna, P. Belser, A. von Zelewsky, *Coord. Chem. Rev.,* 1988, **84,** 85.

54. E.M. Kober, J.L. Marshall, W.J. Dressick, B.P. Sullivan, J.V. Caspar, T.J. Meyer, *Inorg. Chem.,* 1985, **24,** 2755.

55. J. Zhuang, W. Li, W. Su, Y. Liu, Q. Shen, L. Liao, M. Zhou, *Org. Electron.,* 2013, **14,** 2596.

56. A. M. Brouwer, *Pure Appl. Chem.*, 2011, **83**, 2213.

57. C.M. Elliot, E.J. Hershenhart, *J. Am. Chem. Soc.,* 1982, **104,** 7519.

58. Y. Kawanishi, N. Kitamura, S. Tazuke, *Inorg. Chem.,* 1989, **28,** 2968.

59. R.F. Beeston, W.S. Aldridge, J.A. Treadway, M.C. Fitzgerald, B.A. DeGraff, S.E. Stizel, *Inorg. Chem.,* 1998, **37,** 4368.

60. T. Smith, J. Guild, *Trans. Opt. Soc.,* 1931, **33,** 73.

61. W.D. Wright, *Trans. Opt. Soc.,* 1929, **30,** 141.

62. CIE-Datatables <http://www.cie.co.at/publ/abst/datatables15_2004/x2.txt; http://www.cie.co.at/publ/abst/datatables15_2004/y2.txt; http://www.cie.co.at/publ/abst/datatables15_2004/z2.txt> Accessed in November, 2014.

63. A.B.P. Lever, *Inorg. Chem.,* 1990, **29,** 1271,

64. S.S. Fielder, M.C. Osborne, A.B.P. Lever, W.J. Pietro, *J. Am. Chem. Soc.,* 1995, **117,** 6990.

65. L.A. Worl, R. Duesing, P. Chen, L.D. Ciana, T.J. Meyer, *J. Chem. Soc. Dalton Trans.,* 1991, 849.

66. A. Juris, V. Balzani, F. Barigelletti, S. Campagna, P. Belser, A. von Zelewsky, *Coord. Chem. Rev.,* 1988, **84,** 85

67. J.V. Caspar, B.P. Sullivan, T.J. Meyer, *Inorg. Chem.,* 1984, **23,** 2104.

68. E.M. Kober, J.L. Marshall, W.J. Dressick, B.P. Sullivan, J.V. Caspar, T.J. Meyer, *Inorg. Chem.,* 1985, **24,** 2755.

69. C.-L. Ho, H. Li, W.-Y. Wong, *J. Organomet. Chem.,* 2014, **751,** 261.

70. F. Dumur, M. Lepeltier, H.Z. Siboni, P. Xiao, B. Graff, J. Lalevée, D. Gigmes, H. Aziz, *Thin Solid Films,* 2014, **562,** 530.

71. J. Wang, J.; X. Xu, Y. Tian, C. Yao, L. Li, *Synth. Met.,* 2014, **197,** 90.

72. Y. Qi, X. Wang, M. Li, Z. Lu, J. Yu, *JOL,* 2014, **155,** 47.